Research paper

Numerical study of combustion and convective heat transfer of a Mach 2.5 supersonic combustor

CrossMark

Xi Wang, Fengquan Zhong[*], Hongbin Gu, Xinyu Zhang

State Key Laboratory of High Temperature Gas Dynamics, Institute of Mechanics, Chinese Academy of Sciences, China

HIGHLIGHTS

- Convective heat transfer of supersonic combustor was numerically studied.
- Peaks of wall heat flux at varied fuel/air ratios are identified.
- Shock structures and vortices are related to flow separation caused by combustion.

ARTICLE INFO

ABSTRACT

In this paper, characteristics of combustion and convective heat transfer of a supersonic combustor at two fuel/air equivalence ratios of 0.9 and 0.46 were numerically studied. The numerical method of Favre averaged Navier–Stokes simulation with SST k-ω turbulence model and a multiple-step reaction mechanism of ethylene is introduced. The inlet Mach number of the combustor is 2.5 and inlet total temperature is 1650K, corresponding to Mach 6 flight conditions. Ethylene is injected at two locations upstream of a flame-holding cavity. The numerical method was validated by comparing the present results of wall pressures and heat fluxes to experiments and theoretical analysis. It is found that, due to injection of fuel at the bottom wall, fuel/air mixing and combustion occurs mainly in the vicinity of the bottom wall. High non-symmetry in distributions of the bottom and the top wall heat fluxes is observed. Peaks of wall heat flux at different locations and at varied fuel/air equivalence ratios are identified, which are caused respectively by effect of cavity and by shock structure formed upstream of the injection points. It is also found that heat flux peaks are strongly related to the reaction step of $CO \rightarrow CO_2$, contributing to major heat releasing.

1. Introduction

Thermal protection is one of the key technologies for successful scramjet operations. The combustor of scramjet has the most severe thermal environment. For example, the maximum total temperature of combustor may exceed 3000K at a flight Mach number of 6, and the wall heat flux would exceed 3 MW/m² [1].

It is known that convective heat transfer and heat loading on the combustor wall are mainly determined by flow field and combustion properties. Many physical processes including fuel injection and mixing, chemical reaction and heat releasing, shock train structure and its interaction with turbulent boundary layer, may affect wall heat flux, leading to highly non-uniform distributions along the main flow and the circumferential directions. The high non-uniformity in the wall heat flux imposes difficulties in design and optimization of thermal protection such as active cooling for supersonic combustor [2,3]. Therefore, it is imperative to study characteristic of convective heat transfer and wall heat flux at typical flow conditions for scramjet applications.

The direct and conventional measurement of wall heat flux is using high-temperature heat flux gage [4,5]. Another method is to measure time evolution of wall temperatures and interpret the temperature data to the wall heat flux via unsteady heat analysis [6,7]. Besides experiment works about heat flux measurement as mentioned in Refs. [4–7], other related works about wall heat flux of supersonic combustor are reported. Sanderson et al. [8] measured wall heat flux using surface thermocouple sensor.

* Corresponding author. No.15 Beisihuanxi Road, 100190, Beijing, China. Fax: +86 10 82544041.
  E-mail address: fzhong@imech.ac.cn (F. Zhong).

Vincent et al. [9] obtained surface heat flux and temperature of Zirconia-coated copper wall via water-cooled heat flux gage and sub-surface temperature measurement for HIFiRE Direct Connect Rig. Kennedy et al. [10] applied Direct Write Technology for the measurement of heat flux of a direct-connect hydrocarbon-fueled scramjet combustor.

Those methods can only obtain heat fluxes at several points on the wall and lack of fine spacing resolution because of relatively large size of gages. However, numerical study with high accuracy is capable to obtain distributions of wall heat flux and to identify clearly local heat flux peaks. The numerical simulation also provides details of reacting flow field for better understanding of convective heat transfer of supersonic combustor.

In this paper, combustion and convective heat transfer characteristics of a supersonic combustor with inlet Mach number of 2.5 and inlet total temperature of 1650K were numerically studied. The computational method is to solve Favre averaged Navier—Stokes equations (FANS) with SST k-ω turbulence model and a multiple-step reaction model of ethylene. In the next section, numerical method and computational domain are introduced, followed by numerical validations. Results of the combustor flow and wall heat flux at two typical fuel/air equivalence ratios are then presented. Finally, conclusions based on the present results are given.

2. Numerical methods

The configuration of Mach 2.5 supersonic combustor is shown in Fig. 1. The height and width of the combustor inlet cross-section are 40 mm and 85 mm respectively. The total length of the combustor is 1419 mm including an isolator with constant cross section and a length of 395 mm, three divergent sections with angles of 1.5°, 2.0°, 5° at the bottom wall. As shown in the figure, there are two injection locations (Φ1, Φ2), of which, the upstream one is the main injection point. A cavity is installed downstream of the injections, which has a length-to-height ratio of 5.5. The fuel is ethylene and as shown in Table 1, the fuel/air equivalence ratios at two injections are 0.36/0.1 or 0.8/0.1. The total temperature of air at the inlet is 1650K, and the inlet Mach number is 2.5. The thermal boundary of the combustor wall is set to be a constant temperature of 1000K. The reason is that the long run combustor usually operates under regenerative cooling conditions at which the wall temperature is kept to be approximately 1000K [5,11]. The non-reflecting boundary condition is a commonly used outlet B.C. for supersonic flow based on characteristic analysis as described in the literature [12].

The computational domain is half of the combustor due to symmetry in the spanwise direction (z direction in Fig. 1) and the total mesh for computational domain are 3.3 million. The gird numbers in the normal and streamwise directions are changed to study the grid independence. It is found that 90 grids in the normal direction, 500 grids in the streamwise direction, 60 girds in the spanwise direction and 700,000 grids in the cavity are sufficient to

Table 1
Boundary conditions for computational domain.

Mach number at combustor inlet	2.5
Total temperature of air at combustor inlet	1650K
Wall temperature	1000K
Fuel/air equivalence ratio at injector Φ1	0.36/0.8
Fuel/air equivalence ratio at injector Φ2	0.1

obtain an accurate result. Parallel computation based on MPI algorithm is applied to accelerate the computation. It is noted that the first grid point from the wall is at $\Delta y^+ \leq 1$ and there are at least 10 grid points below $y^+ = 10$ for a good mesh resolution to simulate near-wall turbulent flow. The grids are structured except that in the vicinity of the fuel injectors with circular injection holes. The number of unstructured girds is 160,000 and very small compared to the total grids.

It is worthy noticing that the Favre averaged wall heat flux with low frequency properties can be obtained by FANS method and fluctuations of wall heat flux caused by turbulence small scales with high frequencies would be lost. However, it is known that for metallic wall of the combustor, fluctuations of wall heat flux is not a critical issue as regarded in the applications of ceramic wall. Besides, FANS has advantages of good computational stability and high efficiency in solving engineering problems. Therefore, in this paper, FANS is adopted to simulate reacting flow field to investigate the spatial distribution of wall heat flux of supersonic combustor. The governing equations including continuity, momentum and energy equations are averaged to obtain FANS equations:

Continuity equation:

$$\frac{\partial \overline{\rho}}{\partial t} + \frac{\partial}{\partial x_i}\left(\overline{\rho}\widetilde{u}_i\right) = 0 \tag{1}$$

Momentum equation:

$$\frac{\partial}{\partial t}\left(\overline{\rho}\widetilde{u}_i\right) + \frac{\partial}{\partial x_j}\left(\overline{\rho}\widetilde{u}_j\widetilde{u}_i\right) = -\frac{\partial}{\partial x_j}\left(\overline{\rho}\delta_{ij}\right) + \frac{\partial}{\partial x_j}\left(\widetilde{\tau_{ji}^{tot}}\right) \tag{2}$$

Energy equation:

$$\frac{\partial}{\partial t}\left(\overline{\rho}\widetilde{e}_0\right) + \frac{\partial}{\partial x_j}\left(\overline{\rho}\widetilde{u}_j\widetilde{e}_0\right) = -\frac{\partial}{\partial x_j}\left(\widetilde{u}_j\overline{p}\right) - \frac{\partial}{\partial x_j}\left(\widetilde{q_j^{tot}}\right)$$
$$+ \frac{\partial}{\partial x_j}\left(\widetilde{u}_i\widetilde{\tau_{ij}^{tot}}\right) + \widetilde{S}_J + \widetilde{S}_h \tag{3}$$

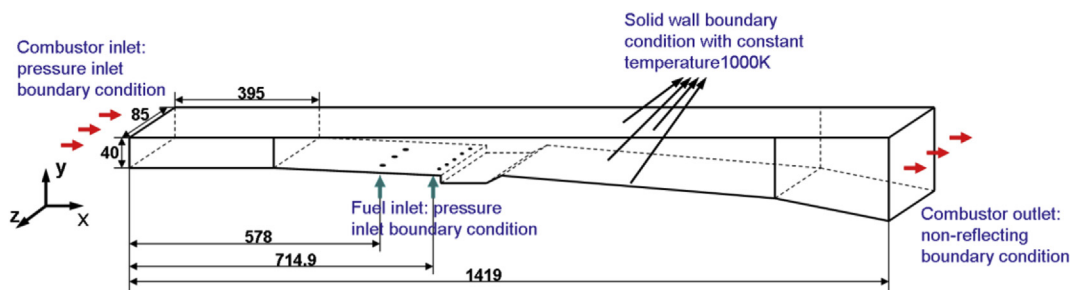where, density weighted time averaging (Favre averaging) is defined as follows:

Fig. 1. Schematic diagram of a Mach 2.5 combustor with boundary conditions (Unit: mm).

Table 2
Reaction model.

	Reaction	Reaction rate	A	Ea (J/kmol)
1	$C_2H_4 + 2O_2 \rightarrow 2CO + 2H_2O$	$Ae^{-Ea/RT}[\chi_{C_2H_4}]^{0.1}[\chi_{O_2}]^{1.65}$	1.12×10^{10}	1.26×10^8
2	$CO + 0.5O_2 \rightarrow CO_2$	$Ae^{-Ea/RT}[\chi_{CO}]^1[\chi_{H_2O}]^{0.5}[\chi_{O_2}]^{0.25}$	2.24×10^{12}	1.67×10^8
3	$CO_2 \rightarrow CO + 0.5O_2$	$Ae^{-Ea/RT}[\chi_{CO_2}]^1$	5×10^8	1.67×10^8

$$\tilde{\Phi} = \overline{\rho\Phi}/\overline{\rho} \tag{4}$$

$$\Phi^{''} = \Phi - \tilde{\Phi} \tag{5}$$

and $\widetilde{e_0} = \tilde{e} + \widetilde{u_k u_k}/2 + k$, turbulent energy $k = \widetilde{u_k^{''} u_k^{''}}/2$, $\widetilde{\tau_{ij}^{tot}} = \widetilde{\tau_{ij}} - \overline{\rho u_i^{''} u_j^{''}}$, $\widetilde{q_j^{tot}} = \widetilde{q_j^{lam}} + \widetilde{q_j^{turb}} = \widetilde{q_j} + C_p\overline{\rho u_j^{''} T}$ for perfect gas which is a reasonable assumption for internal flow with chemical reaction in supersonic combustor, $\overline{p} = (\gamma - 1)\overline{\rho}(\widetilde{e_0} - \widetilde{u_k u_k}/2 - k)$, $\widetilde{S_j}$ represents energy transfer due to species diffusion and $\widetilde{S_h}$ denotes heat release of combustion reaction.

Finite volume method provide by the density based solver of Fluent 6.3 is used to solve the Favre averaged N−S equations and the transport equations of species. The AUSM flux-splitting [13] with 2nd-order upwind scheme is applied for spatial discretization of the convective terms. Viscous fluxes are approximated by a 2nd-order central scheme and the time advancement is calculated by Euler method. The SST k-ω model with compressibility and low Reynolds number corrections [14] is employed for simulation of turbulence. The turbulent kinetic energy, k can be calculated by the turbulence intensity with the following equation:

$$k = \frac{3}{2}(\overline{U}_{inlet}I)^2$$

where, $\overline{U}_{inlet}$ is the mean streamwise velocity at the inlet. The turbulent intensity, I, is determined by the Reynolds number:

$$I = 0.16(\text{Re})^{-1/8}$$

where, Re is Reynolds number based on the inlet flow parameters and hydraulic diameter of the combustor entrance.

The specific dissipation rate, ω is determined as follows,

$$\omega = \rho\frac{k}{\mu}\left(\frac{\mu_t}{\mu}\right)^{-1}$$

where, the ratio of turbulent viscosity to molecular viscosity, μ_t/μ is set to be 10, and ρ, μ are estimated based on the inlet flow parameters.

The perfect gas assumption is used and two 4th-order polynomials as function of temperature based on NIST database are applied to calculate specific heats in temperature ranges of 300K−1000K and of 1000K−5000K respectively. Viscosity and
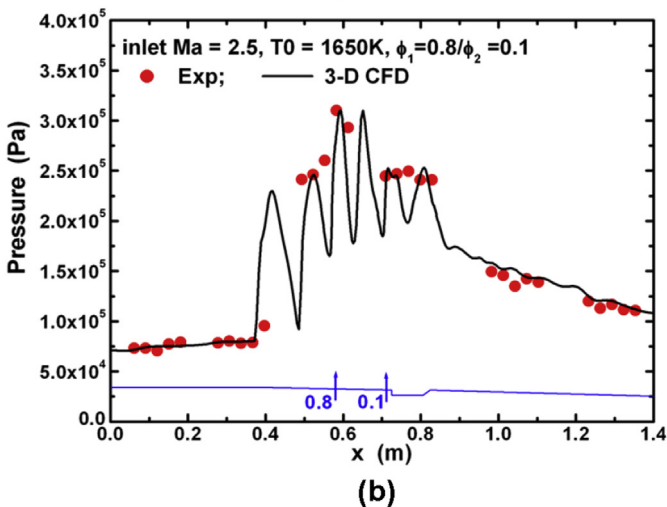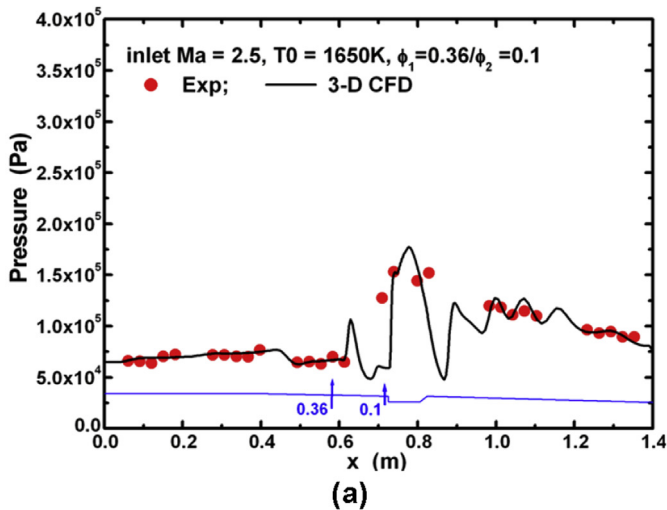

Fig. 2. Comparison of wall pressures obtained with the present computation and experiments.
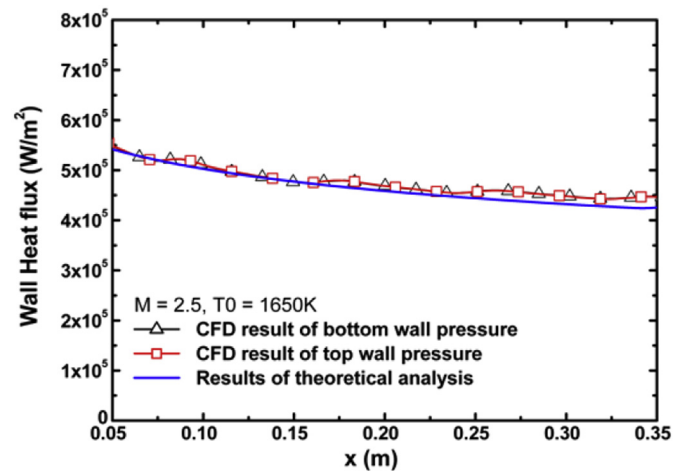

Fig. 3. Comparison of wall heat flux of the isolator by computation and by theoretical analysis.
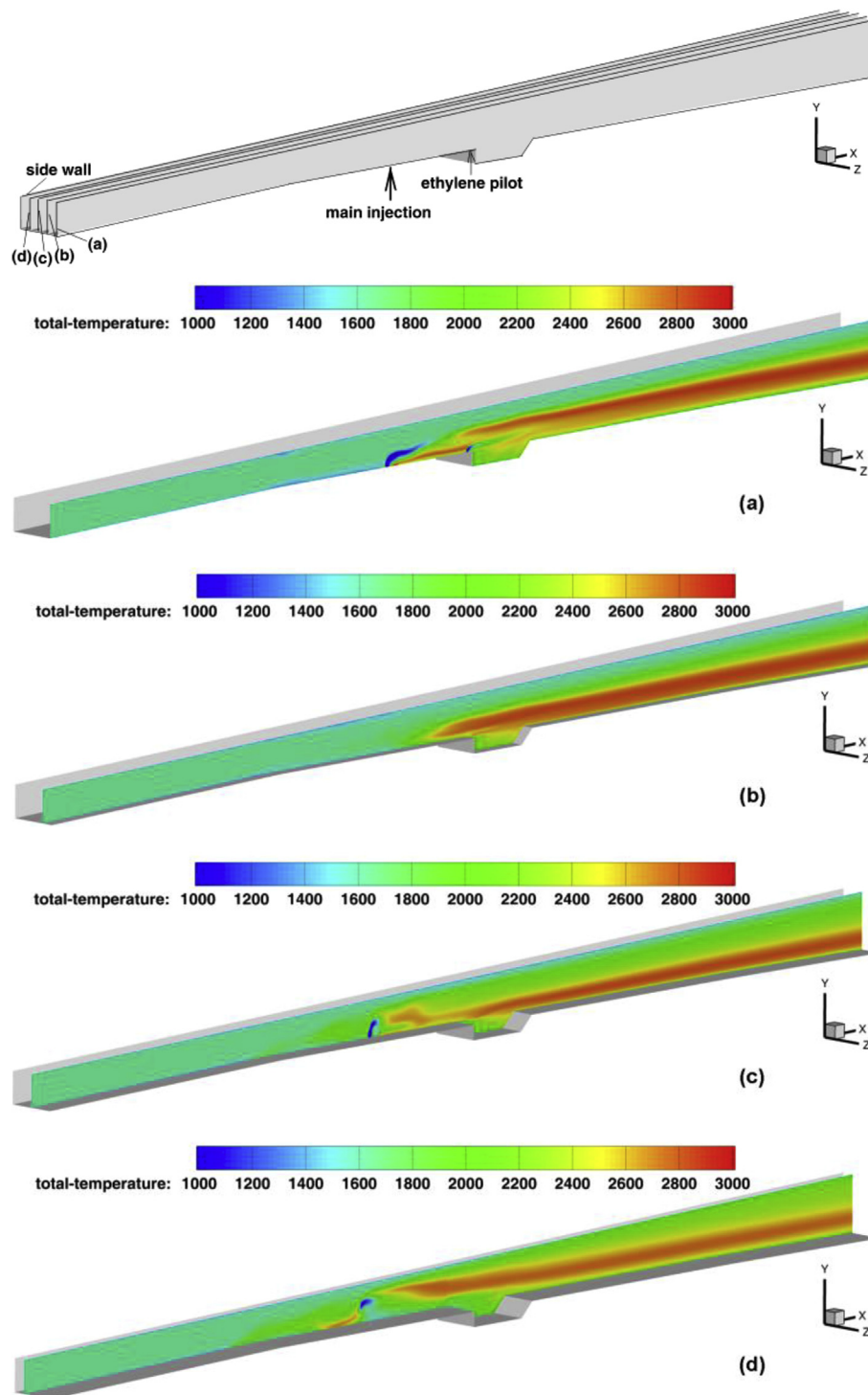
Fig. 4. Contours of total temperature at different x–y planes of the combustor (Unit: K) (Φ = 0.9). a: z = 42.5 mm, b: z = 31.875 mm, c: z = 21.25 mm, d: z = 10.625 mm.
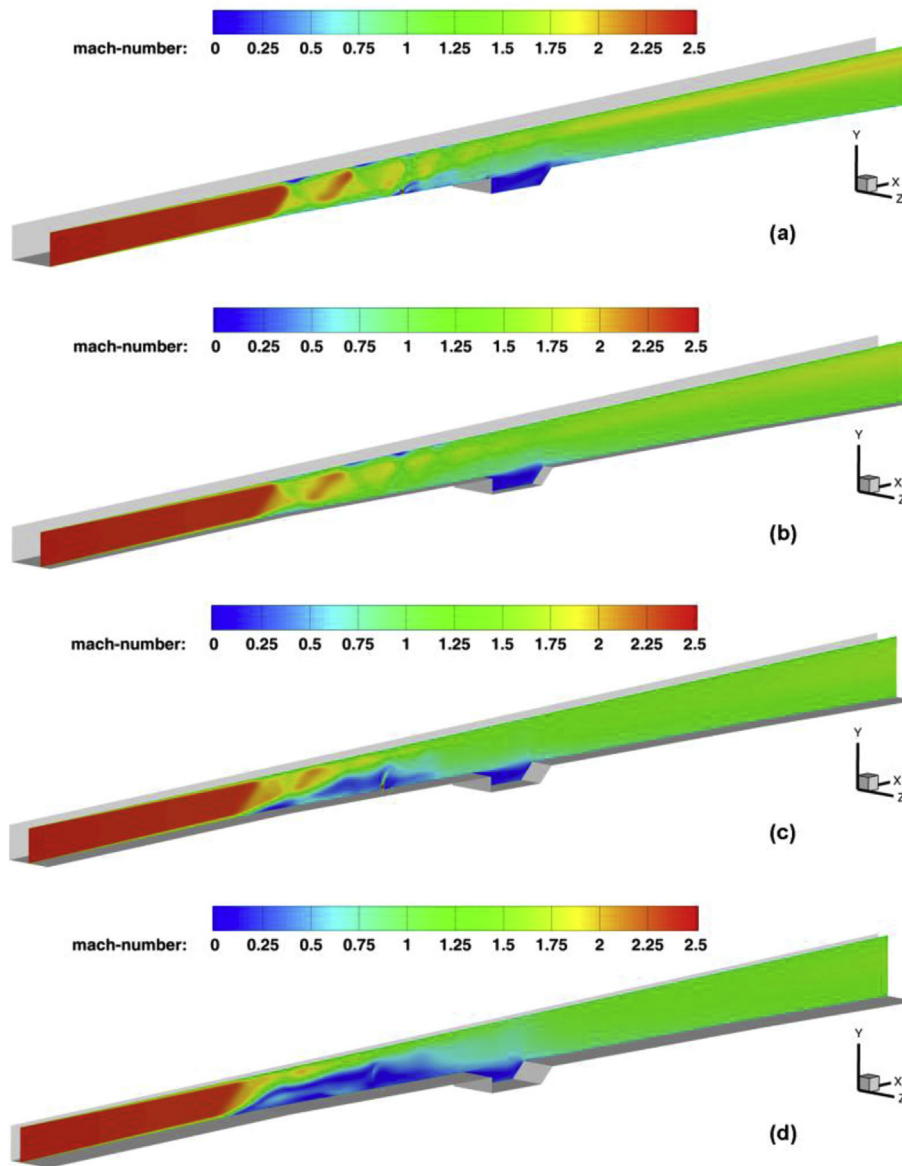
Fig. 5. Contours of Mach number at four different x-y planes of the combustor ($\Phi = 0.9$).

thermal conductivity of species are calculated by kinetic theory with pre-given Lennard-Jones characteristic length and energy parameter. Mass diffusions are determined by the Fick's law and a turbulent Schmidt number is set as 0.7.

A three-step reaction model of ethylene, proposed by Westbrook and Dryer [15], is used to simulate combustion. The species, steps and reaction rate constants are given in Table 2. The model has been examined to be good at prediction of flame speed, heat releasing and CO/CO_2 ratio. For the present study, after ignition, the combusted flow and shock waves are fully developed and the flow field is quasi-steady. The interaction of turbulence and combustion is modeled by a combination of laminar finite-rate model and eddy-dissipation model (EDM) as used in the literature [16,17]. The reaction rate is determined by the smaller one between the Arrhenius rate of laminar finite-rate model and the mixing rate of EDM. It is worthy noticing that residuals of k and omega are found to decrease by 4 orders of magnitude as well as velocity and mass fraction of species. Therefore, it is believed the calculation below converges. Distributions of wall pressure and total temperature at different times are compared to show the time development of combustion flow. If pressure and total temperature curves are found not to change with time, the calculation is then stopped since steady state had been developed.

3. Validations for numerical methods

Fig. 2(a) and 2(b) plot distributions of the top-wall pressure obtained with the present computation and experiments for fuel/air equivalence ratio of 0.46 and 0.9. The experiments were conducted via direct connect supersonic combustion facility at the same flow and fuel conditions. More details of the facility and pressure measurements can be found in our previous experimental
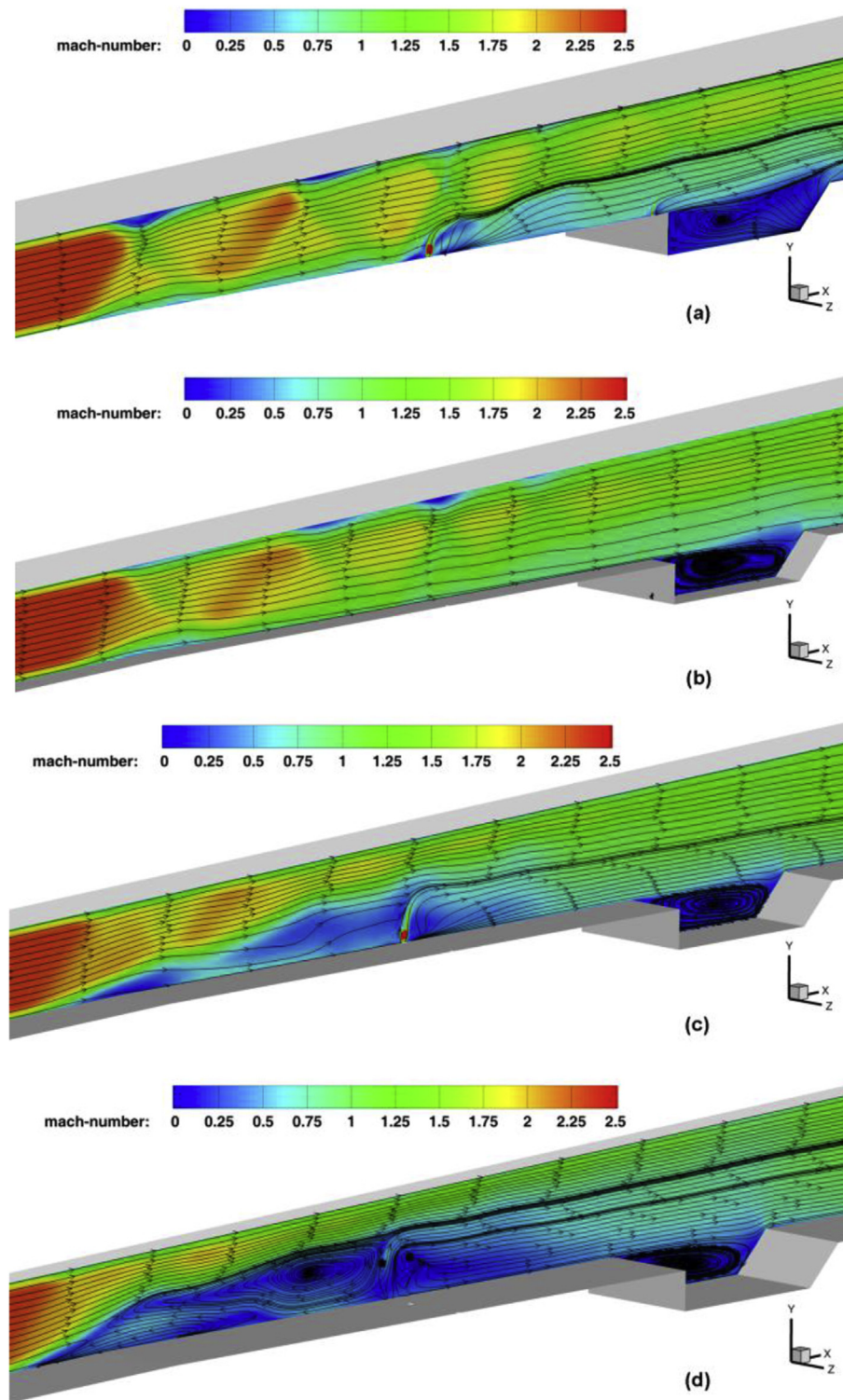
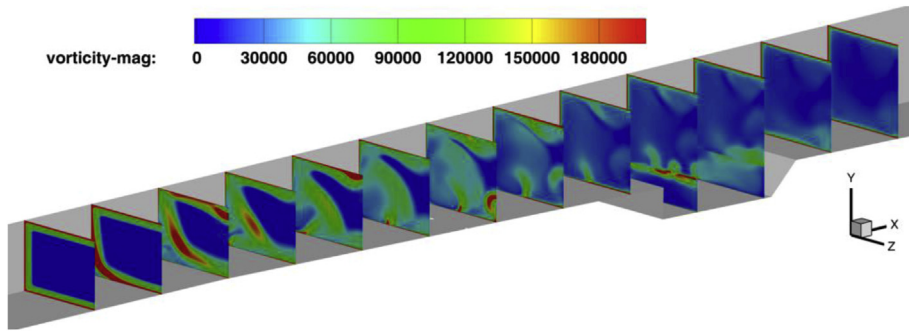**Fig. 6.** Streamline distributions at different x-y planes of the combustor ($\Phi = 0.9$).

Fig. 7. Contours of vorticity at varied cross-section planes for the case of $\Phi = 0.9$.
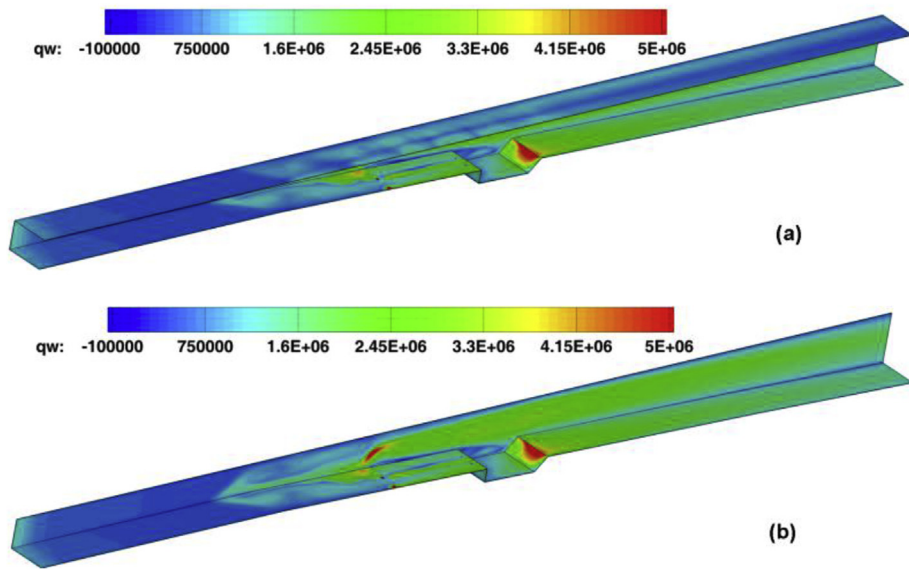

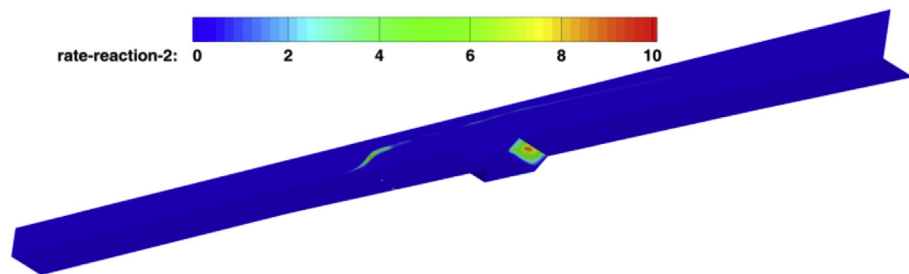**Fig. 8.** Heat flux distributions of the combustor walls (Unit: W/m^2) ($\Phi = 0.9$).

Fig. 9. Contours of reaction rate for $CO \rightarrow CO_2$ on the sidewall and the bottom wall ($\Phi = 0.9$).
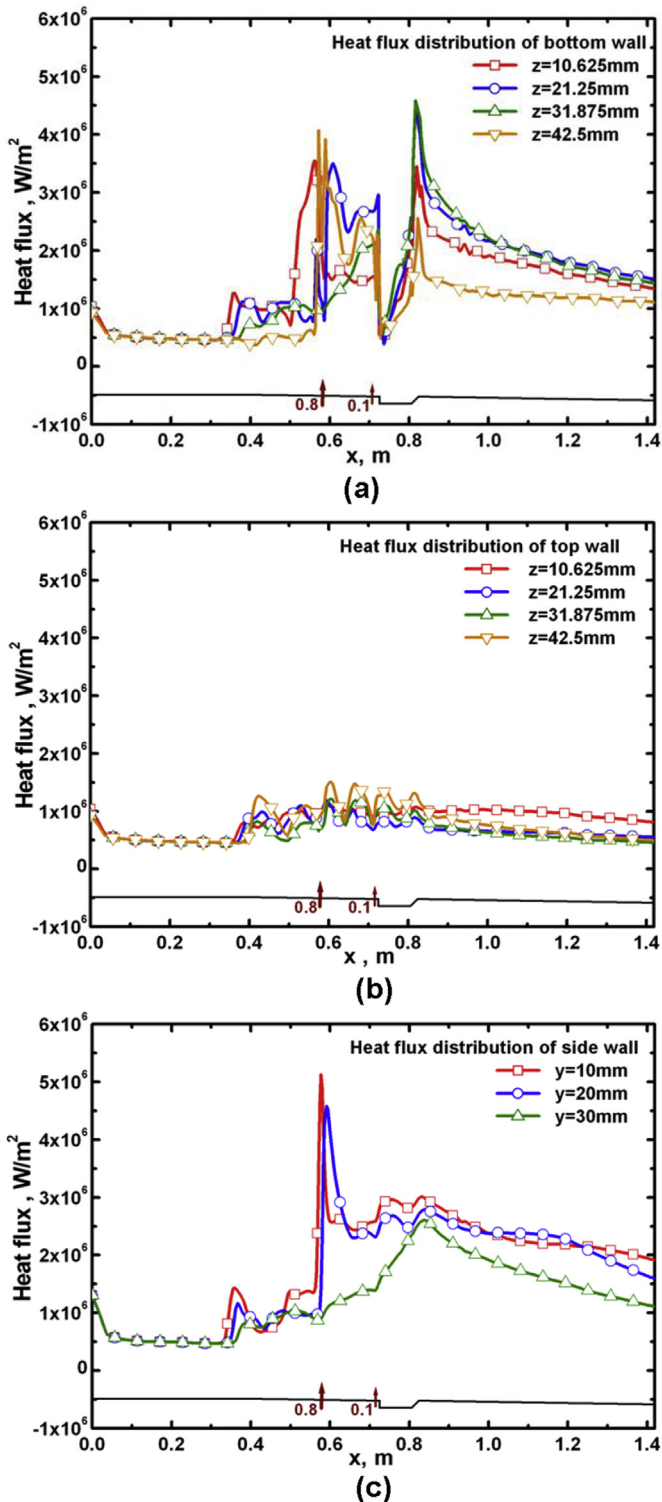
Fig. 10. Distribution of wall heat flux along the x direction at different spanwise locations (a): on the bottom wall, (b): on the top wall and at different heights (c): on the side wall ($\Phi = 0.9$).

work [18,19]. For both cases, the numerical results agree well with the experimental data indicating good accuracy of the present simulation for fuel mixing and reaction.

Due to lack of experimental data of measured wall heat flux at the similar flow and fuel conditions, distribution of wall heat flux in the isolator and upstream of the injections ($x \leq 395$ mm) is used for

the validation of numerical method. The combustion does not occur in this region and the flow is characterized by supersonic boundary layer as described in the literature of [20]. Fig. 3 plots distributions of the top wall and the bottom wall heat flux obtained by the computation as well as a theoretical result obtained with the assumption of supersonic boundary layer flow and Eckert reference enthalpy method [21]. A good agreement is observed in the figure with the maximum discrepancy of only 5%.

4. Results and conclusions

4.1. Results at a high fuel/air equivalence ratio of 0.9

Fig. 4(a)–(d) give contours of total temperature in the x–y planes at varied spanwise locations from the centerline of the combustor to the side wall as indicated in Fig. 4. As shown in the figures, high-temperature regions are located near the combustor bottom wall from where ethylene is injected and burnt. An interesting phenomenon is that part of the high-temperature regions is found upstream of the injection points as indicated in Fig. 4(d) which is the closest one to the combustor side wall. It is due to the local separation flow and shock structures as discussed later by analyzing the Mach number contours as given in Fig. 5 and Fig. 6.

It is clearly seen from Fig. 5 that shock train structures are formed upstream of the injection point and in the isolator to match the pressure difference from the combustor inlet to the injection locations. Shock train structure with boundary layer separation is one of the dominant flow phenomena in dual-mode supersonic combustor and has been observed in many of previous experiments [22,23] or numerical works [24]. As shown in Fig. 5(c) and (d), low velocity areas (blue color) (in the web version) are observed just upstream of the injectors and near the side wall. In addition, streamlines near the injection points and in the cavity in the same x-y planes are plotted in Fig. 6(a)–(d). From Fig. 6(a) to Fig. 6(d), flow separation upstream of the injections becomes more severe as the x-y plane approaching the side wall. As shown in Fig. 6(d), a significant vortical structure is detected upstream of the injections where significant flow separation occurs due to shock/boundary layer interaction and side wall effect. As we know that flow separation leads to low flow velocity and high static temperature that would accelerate combustion process. As part amount of fuel is rolled upstream of the injections due to large vortices as observed in Fig. 6(d), the fuel can mix with air efficiently and burn rapidly, leading to a local high-temperature region as observed in Fig. 4(d).

Fig. 7 gives the contours of vorticity in different y-z planes along the combustor for the case of $\Phi = 0.9$. As shown in the figure, significant vorticity has been identified in three locations: 1) in the corner of the bottom and the side walls upstream of the fuel injections due to flow separation, 2) near the fuel injections due to fuel/air interaction, 3) in the shear layer of the cavity.

Distributions of wall heat flux are presented in Fig. 8(a) (with top wall) and 8(b) (top wall removed). The heat flux on the top wall is considerably lower than that on the bottom and the side wall as a result of fuel injections on the bottom wall of the combustor. As indicated in Fig. 8(b), three regions with local peaks of wall heat flux are identified. One (peak1) is on the backward face of the cavity where large vortex exists and leads to effective mixing and combustion. The second place (peak2) is the corner of the side wall and the bottom wall where significant flow separation occurs as described in Fig. 6(d). The third heat flux peak (peak3) is located in the vicinity of injection hole due to local interaction of fuel jet with incoming flow. It is expected that reaction of $CO \rightarrow CO_2$ with large heat releasing would cause locally large wall heat flux. Fig. 9 shows contours of reaction rate of $CO \rightarrow CO_2$ and no surprisingly, areas

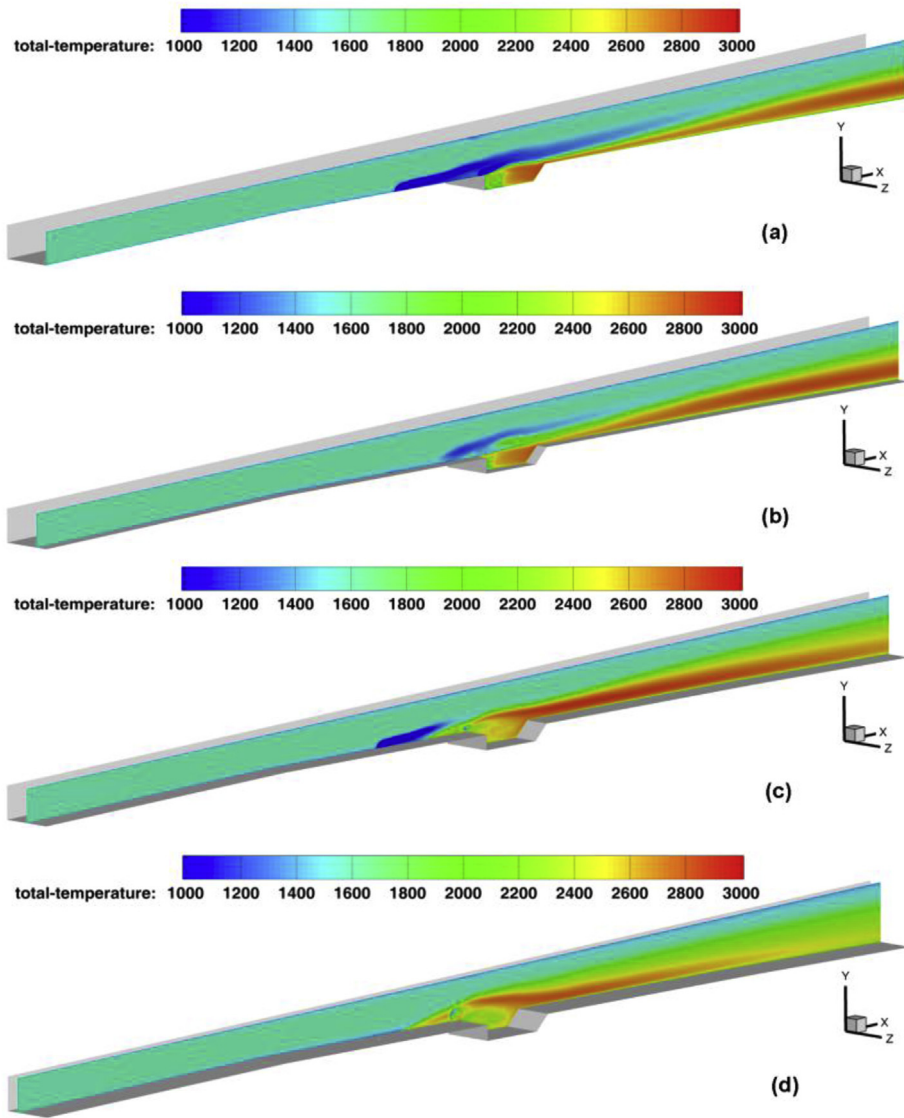**Fig. 11.** Contours of total temperature at different x−y planes of the combustor (Unit: K) (Φ = 0.46) a: z = 42.5 mm, b: z = 31.875 mm, c: z = 21.25 mm, d: z = 10.625 mm.
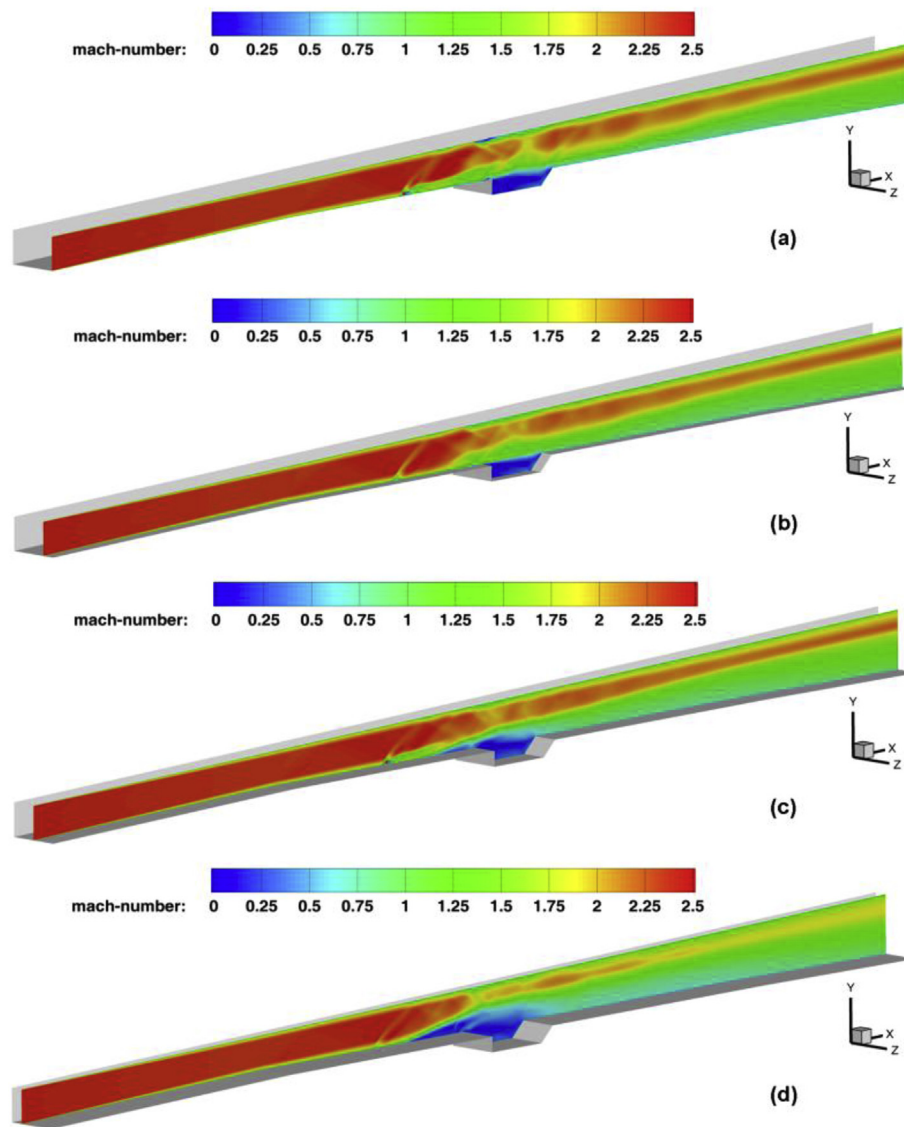
Fig. 12. Contours of Mach number at different x—y planes of the combustor ($\Phi = 0.46$) a: z = 42.5 mm, b: z = 31.875 mm, c: z = 21.25 mm, d: z = 10.625 mm.
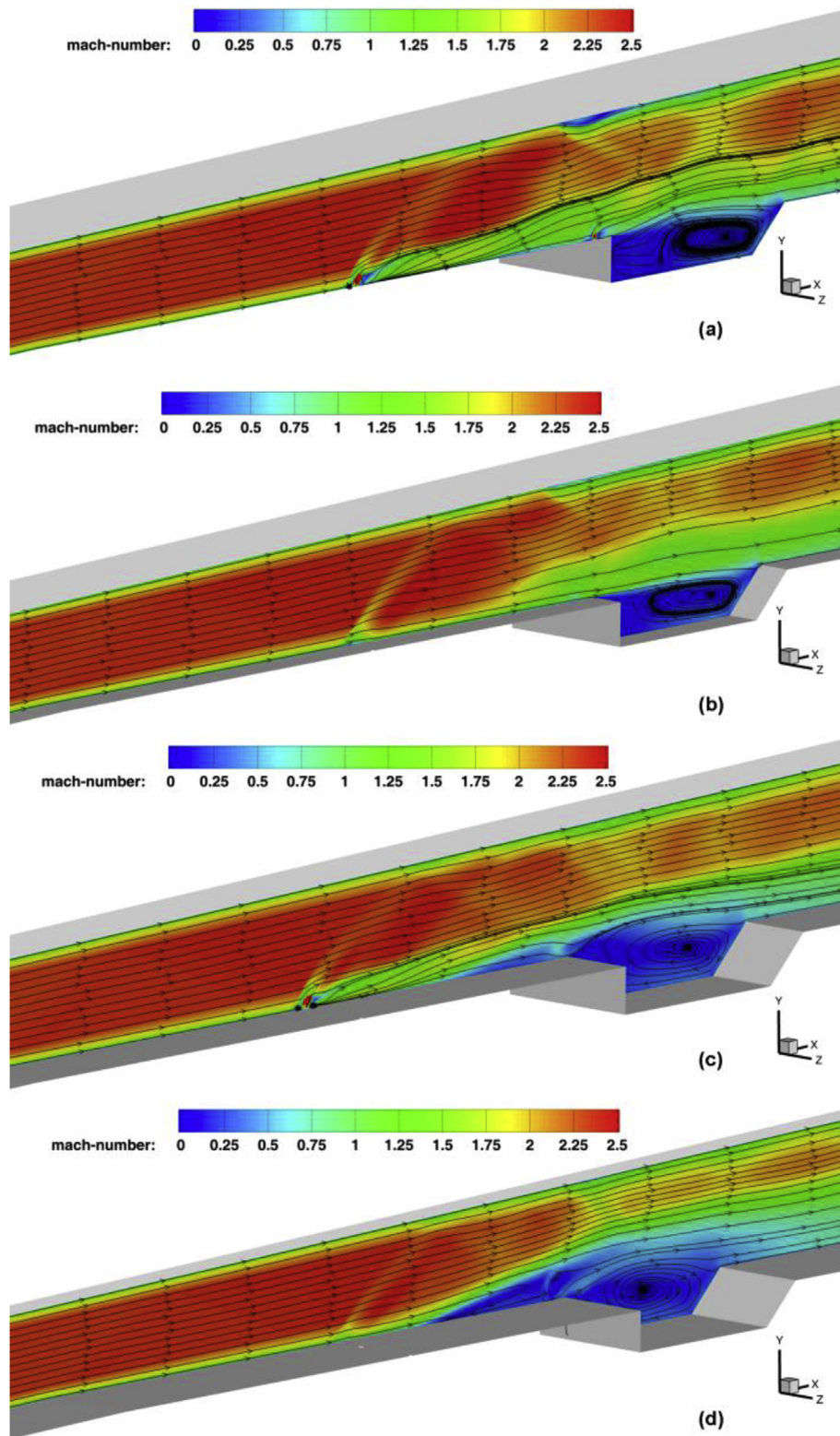
Fig. 13. Streamline distributions at different x–y planes of the combustor ($\Phi = 0.46$).

with maximum reaction rate are consistent with the high heat flux regions.

To study wall heat flux in a more quantitative way, distributions of the bottom wall heat flux along the x direction at varied spanwise positions are plotted in Fig. 10(a). Large variations in the bottom wall heat flux are found at varied spanwise positions. The maximum heat flux may reach 4.5 MW/m^2, much larger than the cross-section averaged value of approximately 1.5 MW/m^2 at the same x location. It indicates that special design and enhancement of cooling should be carefully considered in such regions with
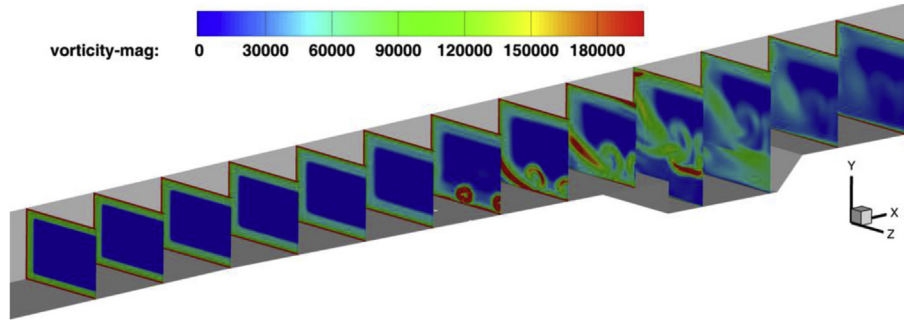
Fig. 14. Contours of vorticity at varied cross-section planes for the case of $\Phi = 0.46$.

significantly high heat flux. Instead, distributions of the top wall heat flux (Fig. 10(b)) are found to be quite uniform and small. No heat flux peaks are observed on the top wall. Fig. 10(c) gives distributions of the side wall heat flux at different heights. In the corner of the bottom and the side walls, a heat flux peak of nearly 5 MW/m² is found, which is consistent to the second heat flux peak as shown in Fig. 8(b).

4.2. Results at a low fuel/air equivalence ratio of 0.46

Fig. 11(a)–(d) give the contours of total temperature for the case of $\Phi = 0.46$. Because of fuel injection at the bottom wall too, the high temperature regions are also located near the bottom wall. Compared to results of the high fuel/air ratio case, no high-temperature region is observed upstream of the injection points as observed in Fig. 4(d). From the Mach number contours in Fig. 12(a)–(d), there are no shock train structures formed in the isolator. Similarly, by looking at streamlines given in Fig. 13(a)–(d), no flow separation is found upstream of the injections. It can be explained by the fact that heat releasing and pressure rise at low fuel/air ratio are not sufficiently large to cause boundary layer separation and to form shock trains in the isolator. The combustion is in a supersonic mode as discussed in the literature of [16,25].

Fig. 14 gives the contours of vorticity in different y-z planes along the combustor for the case of $\Phi = 0.46$. Compare with the result of $\Phi = 0.9$, there is no significant vorticity upstream of the injections as shown in Fig. 3(b) for $\Phi = 0.46$. The vorticity downstream the fuel injection due to fuel/air interaction and in the shear
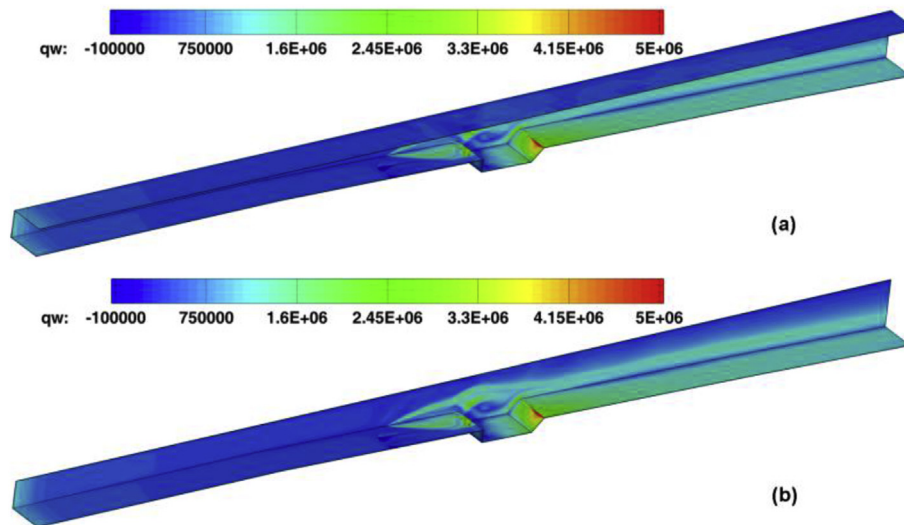

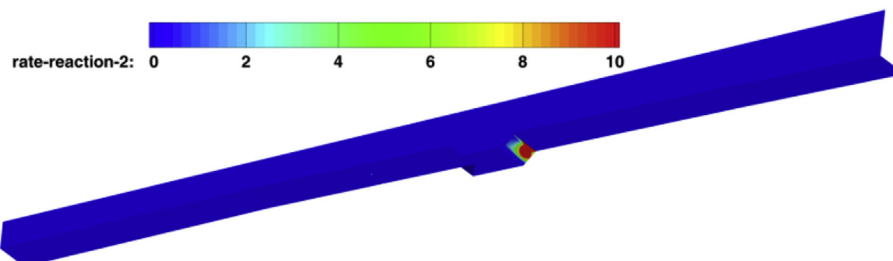**Fig. 15.** Contours of heat flux of the combustor walls (Unit: W/m²) ($\Phi = 0.46$).

Fig. 16. Contours of the reaction rate for $CO \rightarrow CO_2$ on the sidewall and the bottom wall ($\Phi = 0.46$).
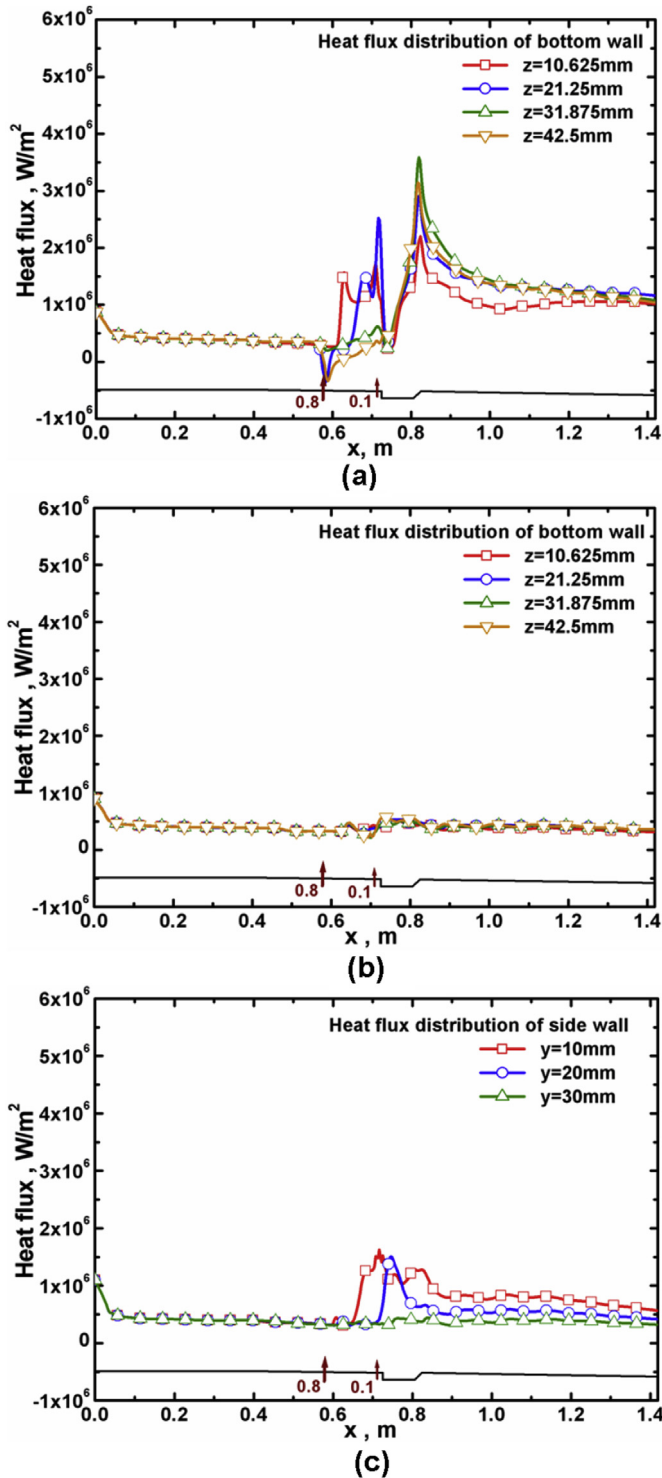
Fig. 17. Distribution of wall heat flux along the x direction at different spanwise locations (a): on the bottom wall, (b): on the top wall and at different heights (c): on the side wall ($\Phi = 0.46$).

layer of the cavity for $\Phi = 0.46$ is obvious and larger than that for the case of $\Phi = 0.9$.

Fig. 15(a) and (b) provide the heat flux contours on the combustor walls with and without top wall. Only one heat flux peak located at the backward edge of the cavity is identified. However, heat flux peak is not found in the corner of the side and the bottom walls as observed in Fig. 8. Fig. 16 gives contours of reaction rate of

the reaction step: $CO \rightarrow CO_2$ and there is only one area with large values of the reaction rate that is located at the backward face of the cavity.

Fig. 17(a)–(c) are distributions of the wall heat flux along the x direction. As shown in Fig. 17(a), the bottom wall heat flux is much lower than that of the case $\Phi = 0.9$. The maximum heat flux is also located at the trailing edge of the cavity with a value of approximately 3.5 MW/m^2, much higher than the cross-section averaged value of 0.95 MW/m^2 at the same x location. The side wall heat flux is also much smaller than that at high fuel/air ratio of 0.9 and the maximum heat flux on the side wall is only 1.5 MW/m^2.

5. Conclusions

In this paper, characteristics of combustion and convective heat transfer of a supersonic combustor with inlet Mach number of 2.5 and inlet total temperature of 1650K are numerically studied at two fuel (ethylene)/air equivalence ratios of 0.9 and 0.46. The numerical method and the reaction model are validated by comparing pressure results and wall heat fluxes obtained with the present computation calculation, the experiments and the theoretical analysis. The present study reveals that, due to fuel injection at the bottom wall of combustor, combustion and heat releasing occurs mainly in the vicinity of the bottom wall and large spatial variations in the wall heat flux is observed. A wall heat flux peak is identified at the backward face of the cavity for both fuel/air ratio cases due to the occurrence of major combustion. A second peak is found in the corner of the side and the bottom wall for the high fuel/air ratio of 0.9 since significant flow separation is generated by shock train structures formed in the isolator. The present results also prove that high heat flux region corresponds to the area with sufficient reaction of $CO \rightarrow CO_2$, contributing to the major heat releasing. Numerical study of distributions of wall heat flux at wider range of fuel/air equivalence ratio and with different inlet Mach numbers is being underway as well as further validations of the wall heat flux especially in the combustion region.

References

[1] R.M. Traci, J.L. Farr, T. Laganelli, A thermal management systems model for the NASA GTX RBCC concept, NASA Technical Report, NASA/CR-2002–211587.
[2] D.R. Sobel, L.J. Spadaccini, Hydrocarbon fuel cooling technologies for advanced propulsion, ASME J. Eng. Gas Turbines Power 119 (2) (1997) 344–351.
[3] R.F. Bergholz, B.D. Hitch, Thermal management systems for high Mach air-breathing propulsion, 30th Aerospace Sciences Meeting & Exhibit, AIAA 1992-0515, Jan. 6-9, 1992.
[4] T. Tsuru, S. Tomioka, K. Kudo, A. Murakami, K. Kato, H. Yamasaki, Skin-friction measurements in supersonic combustion flows of a scramjet combustor, 44th AIAA/ASME/SAE/ASEE Joint Propulsion Conference & Exhibit, AIAA 2008-4578, Jul. 21-23, 2008.
[5] L. Long, J. Wang, X.J. Fan, Development of integrated high temperature sensor for simultaneous measurement of wall heat flux and temperature, Rev. Sci. Instrum. 83 (7) (2012) 074901.
[6] K.F. He, W.Q. Qian, Estimation of heat source term in three-dimensional heat conduction problem from temperature measurements, J. Exp. Fluid Mech. 21 (4) (2007) 53–58.
[7] L.W. Cheng, F.Q. Zhong, H.B. Gu, L.H. Chen, X.Y. Zhang, Application of conjugate gradient method for measurements of wall heat flux of supersonic combustor, Asian Joint Conference on Propulsion and Power 2014, Korea, AJCPP2014–106, 2014.
[8] S.R. Sanderson, B. Sturtevant, Transient heat flux measurement using a surface junction thermocouple, Rev. Sci. Instrum. 73 (7) (2002) 2781–2787.
[9] V. Cuda, Jr, N. E. Hass, Heat flux and wall temperature estimates for the NASA Langley HIFiRE direct connect rig, JANNAF 43rd Combustion, 31st Airbreathing Joint Meeting, Dec. 7-11, 2009.

[10] P. J. Kennedy, J. M. Donbar, Heat flux measurements in a scramjet combustor using direct write technology, 17th AIAA International Space Planes and Hypersonic Systems and Technologies Conference, AIAA 2011-2330, Apr. 11-14, 2011.

[11] X. Wang, F.Q. Zhong, L.H. Chen, X.Y. Zhang, A coupled heat transfer analysis with effects of catalytic cracking of kerosene for actively cooled supersonic combustor, J. Propuls. Technol. 34 (1) (2013) 45–51.

[12] K.W. Thompson, Time dependent boundary conditions for hyperbolic systems, J. Comput. Phys. 68 (1987) 1–24.

[13] M.S. Liou, C.J. Steffen Jr., A new flux splitting scheme, J. Comput. Phys. 107 (1993) 23–39.

[14] F.R. Menter, Two-equation eddy-viscosity turbulence models for engineering applications, AIAA J. 32 (8) (1994) 1598–1605.

[15] C.K. Westbrook, F.L. Dryer, Simplified reaction mechanisms for the oxidation of hydrocarbon fuels in flames, Combust. Sci. Technol. 27 (1981) 14–27.

[16] B.F. Magnussen, B.H. Hjertagerial, On mathematical models of turbulent combustion with special emphasis on soot formation and combustion, Symp. Int. Combust. 16 (1) (1977) 719–729.

[17] J. Li, F.H. Ma, V. Yang, C.K. Lin, T.A. Jackson, A comprehensive study of ignition transient in an ethylene-fueled scramjet combustor, 43rd AIAA/ASME/SAE/ASEE Joint Propulsion Conference & Exhibit, AIAA 2007-5025, Jul. 8-11, 2007.

[18] H.B. Gu, L.H. Chen, X.Y. Chang, Experimental investigation on the cavity-based scramjet model, Chin. Sci. Bull. 54 (16) (2009) 2794–2799.

[19] F. Li, X.L. Yu, H.B. Gu, Z. Li, L.H. Chen, X.Y. Chang, Measurement of temperature, velocity and water vapor concentration in a scramjet combustor based on near-infrared diode laser absorption, 17th AIAA International Space Planes and Hypersonic Systems and Technologies Conference, AIAA 2011-2214, Apr. 11-14, 2011.

[20] W.H. Heiser, D.T. Pratt, Hypersonic Airbreathing Propulsion, American Institute of Aeronautics and Astronautics Inc, Washington, DC, 1994.

[21] E.R.G. Eckert, Engineering relations for heat transfer and friction in high-velocity laminar and turbulent boundary layer flow over surfaces with constant pressure and temperature, Trans. ASME 78 (6) (1956) 1273–1283.

[22] P.J. Waltrup, F.S. Billig, Prediction of precombustion wall pressure distributions in scramjet engines, J. Spacecr. Rockets 10 (9) (1973) 620–622.

[23] B.F. Carroll, J.C. Dutton, Characteristics of multiple shock wave/turbulent boundary-layer interactions in rectangular ducts, J. Propuls. Power 6 (2) (1990) 186–193.

[24] P. Lin, G.V.R. Rao, G.M. O'Connor, Numerical analysis of normal shock train in a constant area isolator, 27th AIAA/SAE/ASME/ASEE Joint Propulsion Conference, AIAA 1991-2162, Jun. 24-26, 1991.

[25] D.J. Micka, J.F. Driscoll, Combustion characteristics of a dual-mode scramjet combustor with cavity flameholder, Proc. Combust. Inst. 32 (2009) 2397–2404.